Dirac Cones and Minigaps for Graphene on Ir(111)

I. Pletikosić,[1] M. Kralj,[1,*] P. Pervan,[1] R. Brako,[2] J. Coraux,[3] A. T. N'Diaye,[3] C. Busse,[3] and T. Michely[3]

[1]*Institut za fiziku, Bijenička 46, 10000 Zagreb, Croatia*

[2]*Institut Ruđer Bošković, Bijenička 54, 10000 Zagreb, Croatia*

[3]*II. Physikalisches Institut, Universität zu Köln, Zülpicher Straße 77, 50937 Köln, Germany*

(Received 17 July 2008; published 6 February 2009)

Epitaxial graphene on Ir(111) prepared in excellent structural quality is investigated by angle-resolved photoelectron spectroscopy. It clearly displays a Dirac cone with the Dirac point shifted only slightly above the Fermi level. The moiré resulting from the overlaid graphene and Ir(111) surface lattices imposes a superperiodic potential giving rise to Dirac cone replicas and the opening of minigaps in the band structure.

DOI: 10.1103/PhysRevLett.102.056808 PACS numbers: 73.22.−f, 73.21.Cd, 79.60.−i, 81.05.Uw

Graphene has recently become a material of increasing scientific interest [1,2]. Its honeycomb structure composed of two equivalent triangular carbon sublattices has important consequences for the dynamics of the charge carriers. The π and π^* bands of freestanding graphene are conical in the proximity of the Fermi energy, with the vertices touching exactly at the Fermi level. This allows a mapping of their behavior to a model of massless fermions obeying the Dirac equation, leading to a plethora of new, observed, or predicted phenomena, such as anomalous half-integer quantum Hall effect or the Klein paradox (see, e.g., Ref. [1]). The Dirac character and the large mobility of charge carriers in graphene [3], along with the ability to manipulate conduction through the field effect [4] or doping [5], make graphene potentially a material for future electronics.

Most of the experimental work on the electronic structure of supported graphene has been performed with graphene on SiC [5–10]. Early research related to graphene on transition metal surfaces [11–14] has received renewed interest in the last years as epitaxial graphene layers of high structural quality can be grown [15–21]. Moreover, the electronic interaction of graphene with a metal is not only of fundamental interest. Recent calculations appear to imply that graphene which interacts weakly with a metal will result in a favorable contact with high transmission [22]. The charge carrier properties of graphene on a metal have been studied on only two substrates, Ni(111) [15,16] and Ru(0001) [17–19]. The π bands of graphene strongly hybridize with Ni(111) [16], while the small bonding distance of the first layer of graphene and the absence of vibrational and electronic signatures characteristic of graphene indicate the same on Ru(0001) [18,19].

For the epitaxially grown graphene where the substrate has a different lattice constant, the stiffness of graphene leads to the formation of structures with large superperiodicity. Simulations within the effective-Hamiltonian formalism for graphene subjected to superperiodic potentials suggest that graphene superlattices could be used for tuning the propagation velocity and the density of charge carriers in graphene, which is of practical interest in building graphene based electronic components [23]. The main effect of a superperiodic potential on the band structure is the formation of minigaps at the crossing points of a band and a backfolded band, as found, e.g., for Si(111)-$\sqrt{21} \times \sqrt{21}$-(Ag + Au) [24]. However, minigaps were observed neither in graphene on SiC [8] nor on Ru(0001), where they are expected to be present [18].

Here we report on the investigation of the electronic structure of graphene on Ir(111) by angle-resolved photoelectron spectroscopy (ARPES). We show that graphene exhibits a Dirac cone comparable to that of pristine graphene. Because of the moiré superstructure resulting from the lattice mismatch between graphene and Ir(111), a corresponding superperiodic potential exists which gives rise to the opening of moiré-induced minigaps in the band structure.

The experiments have been performed in two ultrahigh vacuum systems for ARPES in Zagreb and scanning tunneling microscopy (STM) in Cologne with base pressures in the low 10^{-8} Pa range using identical procedures for substrate cleaning and graphene fabrication. Graphene was prepared on the clean Ir(111) surface by 7–15 cycles of room temperature ethene adsorption to saturation and subsequent thermal decomposition at 1450 K. ARPES spectra have been taken at 60 K by a Scienta SES-100 hemispherical electron analyzer with an energy resolution of $\sim$25 meV using 21.22 eV photons from a helium discharge source with a beam spot diameter of about 2 mm. For the parallel momentum scan the polar angle ϑ ranged from 40° to 70°. The azimuthal angle, φ, was changed by a wobble stick and checked by low energy electron diffraction (LEED) spot orientation with the precision of $\pm 0.5°$. Below we show that for a range of azimuths within a few degrees around the Γ-K-M direction, the absolute value of φ can be determined to a precision better than 0.1° when the measured dispersion is fitted by the tight-binding approximation bands of graphene [25].

Graphene on Ir(111) grows with graphene $[11\bar{2}0]$ and Ir $[10\bar{1}]$ directions almost perfectly aligned. Because of the

difference in lattice constants, a (9.32 × 9.32) moiré with a repeat distance of 2.53 nm is formed [21]. The LEED patterns—indistinguishable in appearance in our two setups—display aligned first order diffraction spots of the Ir surface and graphene lattices [arrows in Fig. 1(a)] surrounded by the spots of the moiré. The relative position of the carbon atoms with respect to the iridium surface atoms changes within the moiré cell, giving rise to a contrast in STM with the moiré periodicity [Fig. 1(b)]. The amplitude and sign of the moiré contrast depend on tunneling voltage [21], indicating its largely electronic origin. From images of higher magnification [inset of Fig. 1(b)], which display the moiré contrast together with the graphene lattice, the misalignment of graphene with respect to the substrate is accurately determined. Statistics for ~25% graphene covered surface yield a 0.25° scatter in orientation between the two lattices. STM imaging of the surface covered up to 70% by graphene shows flakes with lateral dimensions ranging from several hundred nanometers to a few micrometers. The structural perfection and insignificant orientation scatter (comparable with the 0.1° angular resolution of our electron analyzer) of graphene are a prerequisite for the successful application of ARPES.

Because of the alignment of the graphene lattice and the Ir(111) surface lattice, their Brillouin zones (BZ) are aligned as well (cf. Fig. 3). The spectrum of clean Ir(111) along Γ-*K*-*M* shown in Fig. 2(a) encompasses a region where the graphene Dirac cone is expected. Conveniently, this region coincides with an energy gap in the Ir(111) electronic structure. Three weakly dispersing states, which we identify as surface states, are clearly visible in the gap: S_1 near the Fermi level, and S_2 and S_3 passing near the low edge of the gap. The ARPES spectrum of graphene on Ir(111), shown in Fig. 2(b), contains all the features required to discuss the essential properties of graphene: (i) presence of a Dirac cone, (ii) marginal doping, (iii) additional bands, and (iv) opening of minigaps. The π band with linear dispersion up to the Fermi level, the Dirac cone, is visible at the graphene *K* point [26]. The π-band spectrum is sharp, with a full width at half maximum not larger than 0.15 eV and 0.035 $Å^{-1}$ in the energy and momentum distribution curves, respectively. The Dirac cone branches have noticeably anisotropic intensity. The measured ARPES π-band dispersion is accurately reproduced for all measured azimuths by the tight-binding approximation bands for the unperturbed graphene described in [25], shifted in energy in order to obtain the best fit of the position of the main and replicated Dirac cones. According to this fit we estimate the position of the Dirac point to be 0.10 ± 0.02 eV above the Fermi energy; i.e., graphene on Ir(111) is just slightly *p* doped. As the Dirac point is not accessible with ARPES, we are unable to judge whether a band gap opens at the Dirac point or not [27]. However, if there is one, it ought to be smaller than twice the distance from the Fermi energy to the estimated Dirac point; i.e., its width must be smaller than 0.20 eV. Besides the primary Dirac cone Fig. 2(b) displays an additional band, a faint replica labeled *R*. At the location where the band *R* intersects the Dirac cone in the Γ-*K* branch [indicated by a horizontal arrow in Fig. 2(b)], a band gap is visible, in the following referred to as minigap. A minigap is also visible in the *K*-*M* branch in the Dirac cone in Fig. 2(b).

In order to clarify the origin of the additional band *R* and the minigaps in Fig. 2(b) we show the Brillouin zones of graphene and Ir(111) in Fig. 3(a). The reciprocal lattice vectors $\mathbf{G}_{\mathrm{Ir}}$ and $\mathbf{G}_g$ of the Ir surface and graphene, respec-

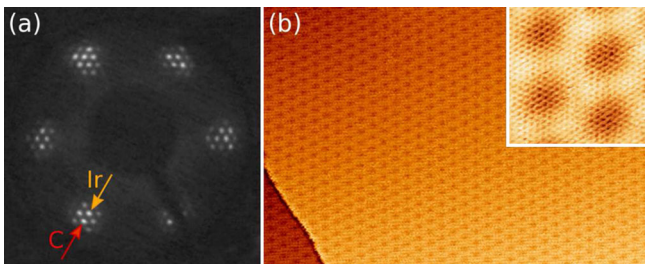

FIG. 1 (color online). (a) LEED pattern (69 eV) of graphene on Ir(111). First order Ir spots, C spots, as well as surrounding moiré spots are visible. (b) STM topograph (75 nm × 50 nm) exhibiting moiré contrast (enhanced by an unsharp masking filter). Tunneling conditions 0.05 V, 32 nA. Inset: 5 nm × 5 nm atomic resolution image of graphene lattice. Tunneling conditions 0.37 V, 32 nA.

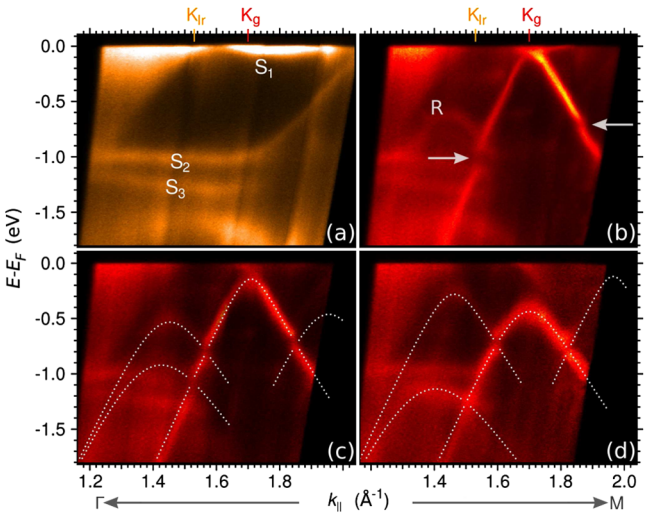

FIG. 2 (color online). (a) ARPES spectrum of clean Ir(111), $\varphi = 0.5° \pm 0.1°$. The positions of *K* points of iridium and graphene are marked as K_{Ir} and K_g, respectively. $S_1 - S_3$ are surface states. (b) ARPES spectrum of Ir(111) covered by graphene along the same azimuth as in (a). Horizontal arrows denote the minigap in the primary Dirac cone. A visible replica band is labeled as *R*. Detailed analysis in [34]. (c), (d) ARPES spectra for $\varphi = 1.4° \pm 0.1°$ and $\varphi = 3.0° \pm 0.1°$, respectively. The dashed lines are tight-binding-approximation-calculated bands for Dirac cones located at positions 0, 1, 2, and 5 defined in Fig. 3(b).

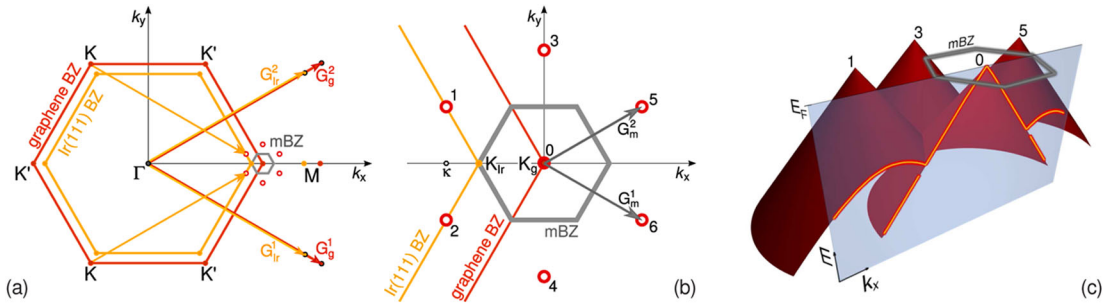

FIG. 3 (color online). (a) BZ of the Ir(111) surface and graphene lattices drawn to scale. Mini–Brillouin zone (mBZ) is indicated around the K point of graphene. Open dots denote the vertices of Dirac cones replicated by moiré reciprocal vectors, $\mathbf{G}_m$. (b) Blowup of the mBZ. Central dot denotes the center of the primary Dirac cone, while 1–6 are replicas. (c) ARPES experimental plane (shaded) along the Γ-K-M high symmetry direction cuts the primary and replica cones (only partially shown). Bright lines at the intersection mark the bands observed in Fig. 2(b).

tively, give rise to the moiré reciprocal vectors $\mathbf{G}_m = \mathbf{G}_g - \mathbf{G}_{\mathrm{Ir}}$, the same which create the LEED pattern in Fig. 1(a). From the dependence of the moiré contrast on tunneling parameters [21] it is evident that the electron potential of graphene is modulated by the substrate. This superperiodic potential, with the corresponding $\mathbf{G}_m$ vectors, creates replica bands centered at the points labeled 1–6 in Fig. 3(b) and opens the gap in the Dirac cone along the mini-BZ (mBZ) boundary. For the Γ-K-M experimental scan direction the cones 1 and 2 give rise to the hyperbolic band with the maximum centered at κ [schematically shown in Figs. 3(b) and 3(c)], visible as the band R in Fig. 2(b). As we turn the scan direction off the Γ-K-M, we move away from the vertex of the primary Dirac cone. Its ARPES cut gets lower in energy, while the opposite happens for the replicas whose vertex is approached, as exemplified for two azimuths in Figs. 2(c) and 2(d).

Replica cones in epitaxial graphene may arise as a final state effect through surface umklapp, involving the reciprocal Ir surface lattice vectors $\mathbf{G}^1_{\mathrm{Ir}}$ and $\mathbf{G}^2_{\mathrm{Ir}}$ [cf. Fig. 3(a)] in a momentum change of the photoelectron diffracted at the surface. This mechanism was put forward in explaining the nature of replicas in graphene on SiC(0001) where, contrary to our observation, the replica cone intensity disappeared at room temperature [8]. Consistent with this interpretation no gaps at the intersection of primary and replica cones were observed [7,8]. Thus, the presence of superperiodic contrast in STM topographs of graphene on SiC(0001) is then to be interpreted as a purely geometric height modulation [28]. Though we cannot exclude final state contributions to the intensity of the replica cones, the surface umklapp alone cannot create the minigap reported here. Therefore, we consider the presence of the minigap as an evidence for an initial state effect in ARPES, i.e., the existence of a moiré periodic potential. The analysis of ARPES spectra reveals that the minigap is indeed located on the Bragg planes bounding the mBZ (Fig. 4). The measured gap width is in the range 0.1–0.2 eV. Consequently, the amplitude of the moiré potential is of the order of 0.05–0.10 eV, small compared to the π-band width. No closing of the minigap was observed. Note that a model using a long-wavelength superperiodic potential which does not break the symmetry of the two graphene sublattices opens a minigap which vanishes at specific points of the boundary of the superstructure BZ, but does not open the gap at the Dirac point [23].

The symmetry breaking as a consequence of the inequivalence of two carbon atoms within each unit cell of graphene ought to imply opening of a band gap at the Dirac point [29], and lifting of the complete asymmetry of the ARPES intensity [8,30]. A band gap due to symmetry breaking has been clearly observed in the bilayer and few layer graphene on SiC(0001) [7,8], but it remains under debate for monolayer graphene on the same substrate [9,10]. A detailed analysis of the moiré of graphene on Ir(111) shows that the atoms in the two sublattices of graphene are locally and globally inequivalent [21]. The global inequivalence reveals itself through the fact that Ir clusters formed on graphene [31,32] bind only to the areas

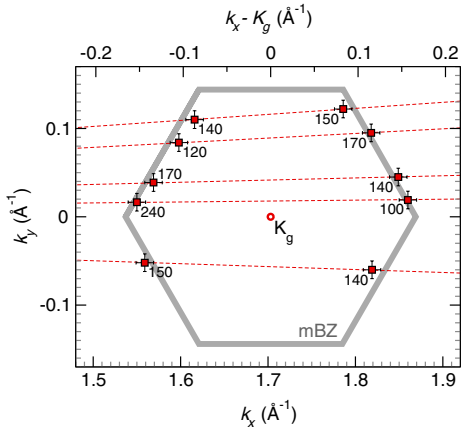

FIG. 4 (color online). The minigaps determined from ARPES scans along the directions indicated by dashed lines fall on the edge of the mini–Brillouin zone. Their widths are annotated in meV. The dashed lines correspond to $\varphi = -1.9°$, $\varphi = 0.5°$, $\varphi = 1.4°$, $\varphi = 3.0°$, and $\varphi = 3.9°$.

of the moiré where the carbon atoms of one sublattice sit atop of substrate iridium atoms. Our ARPES spectra show visible asymmetry of the photoemission intensity, which along with the estimate of a small gap at the Dirac point (<0.2 eV) indicates that the effects of the symmetry breaking for graphene on iridium are small.

As one of the most prominent features, the Dirac cone of graphene on Ir(111) shows no sign of hybridization with substrate electronic bands. Consistently, density functional theory (DFT) calculations taking into account the large supercell of graphene on Ir(111) suggest a weak bonding of graphene [31,32]. In particular, density functional theory calculations yield a large average graphene-Ir(111) separation of 0.34 nm [32], which also explains the defect free growth of the graphene flakes over step edges [20]. Our measurements suggest that the weakness of bonding can be ascribed to the dearth of metallic states of appropriate symmetry (i.e., the existence of the band gap) around the K point of the surface BZ of Ir(111). Marginal p doping comes out as a fortuitous match of several system parameters: proper graphene-Ir(111) distance, work function difference, and weak chemical bonding [33].

Our experiments single out graphene on Ir(111) as a system with unique properties as compared with other epitaxially grown graphene systems. In distinction to graphene on Ni(111) [15,16] and Ru(0001) [17–19], it is a weakly interacting graphene. In distinction to graphene on SiC(0001) [5–10,28,29] and two-layer graphene on Ru (0001) [19], it is a simple system with no carbon rich intermediate layer necessary to passivate the substrate. It is this simplicity, together with its unparalleled structural quality, which makes it an attractive candidate for model experiments. To give an example, for graphene on Ir(111) there is a straightforward method to vary the strength of the moiré periodic potential through ordered adsorption of small metal clusters of well defined size into the moiré [31], allowing one experiments on charge carrier manipulation through periodic potentials [23].

In conclusion, our ARPES measurements show that the electronic bands of graphene on Ir(111) near the Fermi level have the form of the Dirac cone of pristine graphene, only slightly shifted to lower binding energies due to a marginal p doping by the substrate. The periodic potential associated with the moiré gives rise to the formation of replica cones and minigaps at the Bragg planes between the primary and replica cones. The simplicity of the system and its desirable structural and electronic properties make it interesting for fundamental research and a candidate for graphene-metal contacts in potential applications of graphene in electronics.

M. K. and P. P. acknowledge fruitful discussions with T. Valla. Financial support of the Ministry of Science, Education and Sports of the Republic of Croatia through Projects No. 035-0352828-2840 and No. 098-0352828-2836, as well as of DFG through the project ''Two dimensional cluster lattices on graphene moirés'' is acknowledged. J. C. thanks the AvH Foundation for financial support.

*mkralj@ifs.hr

[1] A. K. Geim and K. S. Novoselov, Nature Mater. **6**, 183 (2007).
[2] A. H. Castro Neto *et al.*, Rev. Mod. Phys. **81**, 109 (2009).
[3] K. I. Bolotin *et al.*, Phys. Rev. Lett. **101**, 096802 (2008).
[4] K. S. Novoselov *et al.*, Science **306**, 666 (2004).
[5] A. Bostwick *et al.*, Nature Phys. **3**, 36 (2007).
[6] C. Berger *et al.*, Science **312**, 1191 (2006).
[7] T. Ohta *et al.*, Science **313**, 951 (2006).
[8] A. Bostwick *et al.*, New J. Phys. **9**, 385 (2007).
[9] E. Rotenberg *et al.*, Nature Mater. **7**, 258 (2008).
[10] S. Y. Zhou *et al.*, Nature Mater. **7**, 259 (2008).
[11] S. Hagstrom, H. B. Lyon, and G. A. Somorjai, Phys. Rev. Lett. **15**, 491 (1965).
[12] J. May, Surf. Sci. **17**, 267 (1969).
[13] C. Oshima and A. Nagashima, J. Phys. Condens. Matter **9**, 1 (1997).
[14] N. R. Gall, E. V. Rut'kov, and A. Y. Tontegode, Int. J. Mod. Phys. B **11**, 1865 (1997).
[15] Y. S. Dedkov *et al.*, Phys. Rev. Lett. **100**, 107602 (2008).
[16] A. Grüneis and D. V. Vyalikh, Phys. Rev. B **77**, 193401 (2008).
[17] S. Marchini, S. Günther, and J. Wintterlin, Phys. Rev. B **76**, 075429 (2007).
[18] A. L. Vázquez de Parga *et al.*, Phys. Rev. Lett. **100**, 056807 (2008).
[19] P. W. Sutter, J.-I. Flege, and E. A. Sutter, Nature Mater. **7**, 406 (2008).
[20] J. Coraux *et al.*, Nano Lett. **8**, 565 (2008).
[21] A. T. N'Diaye *et al.*, New J. Phys. **10**, 043033 (2008).
[22] N. Nemec, D. Tománek, and G. Cuniberti, Phys. Rev. B **77**, 125420 (2008).
[23] C.-H. Park *et al.*, Nature Phys. **4**, 213 (2008).
[24] J. N. Crain *et al.*, Phys. Rev. B **66**, 205302 (2002).
[25] S. Reich *et al.*, Phys. Rev. B **66**, 035412 (2002).
[26] Although the shape of the primary Dirac cone is fitted perfectly by the tight-binding calculations discussed later in the text, presently its weak hybridization with the surface state S_1 cannot be excluded.
[27] No conclusion about the existence of the gap at the Dirac point could be drawn from our sodium doping experiments, as the doping shifted the Dirac point below the Fermi level but altered the superstructure of graphene as well.
[28] P. Mallet *et al.*, Phys. Rev. B **76**, 041403(R) (2007).
[29] S. Y. Zhou *et al.*, Nature Mater. **6**, 770 (2007).
[30] H. Daimon *et al.*, J. Electron Spectrosc. Relat. Phenom. **76**, 487 (1995).
[31] A. T. N'Diaye *et al.*, Phys. Rev. Lett. **97**, 215501 (2006).
[32] P. J. Feibelman, Phys. Rev. B **77**, 165419 (2008).
[33] G. Giovannetti *et al.*, Phys. Rev. Lett. **101**, 026803 (2008).
[34] See EPAPS Document No. E-PRLTAO-102-054908 for a thorough analysis of the spectrum in Fig. 2(b). For more information on EPAPS, see http://www.aip.org/pubservs/epaps.html.